[Article] DOI: 10.13208/j.electrochem.2214002 Http://electrochem.xmu.edu.cn

A Co Porphyrin with Electron-Withdrawing and Hydrophilic Substituents for Improved Electrocatalytic Oxygen Reduction

Hong-Bo Guo[#], Ya-Ni Wang[#], Kai Guo, Hai-Tao Lei, Zuo-Zhong Liang[*], Xue-Peng Zhang[*], Rui Cao[*]

(*Key Laboratory of Applied Surface and Colloid Chemistry, Ministry of Education, School of Chemistry and Chemical Engineering, Shaanxi Normal University, Xi'an 710119, China*)

Abstract: Understanding factors that influence the catalyst activity for oxygen reduction reaction (ORR) is essential for the rational design of efficient ORR catalysts. Regulating catalyst electronic structure is commonly used to fine-tune electrocatalytic ORR activity. However, modifying the hydrophilicity of catalysts has been rarely reported to improve ORR, which happens at the liquid/gas/solid interface. Herein, we report on two Co porphyrins, namely, NO_2-CoP (Co complex of 5,10,15,20-tetrakis(4-nitrophenyl)porphyrin) and 5F-CoP (Co complex of 5,10,15,20-tetrakis(pentafluorophenyl)porphyrin), and their electrocatalytic ORR features. By simultaneously controlling the electronic structure and hydrophilic property of the meso-substituents, the NO_2-CoP showed higher electrocatalytic activity than the 5F-CoP by shifting the ORR half-wave potential to the anodic direction by 60 mV. Compared with the 5F-CoP, the complex NO_2-CoP was more hydrophilic. Theoretical calculations suggest that NO_2-CoP is also more efficient than 5F-CoP to bind with an O_2 molecule to form Co^{III}-$O_2^{\bullet-}$. This work provides a simple but an effective strategy to improve ORR activity of Co porphyrins by using electron-withdrawing and hydrophilic substituents. This strategy will be also valuable for the design of other ORR molecular electrocatalysts.

Key words: molecular electrocatalysis; oxygen reduction; Co porphyrin; hydrophilicity; electronic structure

1 Introduction

Electrocatalytic oxygen reduction reaction (ORR) is involved in many new energy conversion and storage techniques, including fuel cells and metal-air batteries[1-8]. The efficiency of ORR at the cathodes of these devices determines their overall efficiency for energy conversion. Therefore, developing efficient ORR electrocatalysts have attracted increasing interests in the past decades. Understanding factors that can influence the catalyst activity is essential for the rational design of efficient ORR catalysts[9]. Metal porphyrins have been extensively studied as ORR electrocatalysts because (1) nature uses heme proteins, such as cytochrome *c* oxidases, to reduce O_2 to water and also (2) the structure of metal porphyrins can be systematically modified to investigate structure-function relationships[10-25]. Among these studied metal porphyrins, Co porphyrins have shown high activity for ORR[26-29]. However, further improving the ORR activity of Co porphyrins is still required.

Currently, there are many reports on improving catalytic ORR activity of Co porphyrins[30-40]. Regulating catalyst electronic structure through ligand substituents is an effective strategy to tune ORR activity[41,42]. It is known that metal porphyrins with electron-withdrawing groups can be easily reduced, leading to lowered ORR overpotentials[43]. For example, we have recently reported that 5F-CoP with four

Cite as: Guo H B, Wang Y N, Guo K, Lei H T, Liang Z Z, Zhang X P, Cao R. A Co porphyrin with electron-withdrawing and hydrophilic substituents for improved electrocatalytic oxygen reduction. *J. Electrochem.*, 2022, 28(9): 2214002.

Received: 2022-04-13, Revised: 2022-05-17. #These authors contributed equally to this work. *Corresponding author, Liang Zuo-Zhong, Tel: (86)15529262976, E-mail: liangzuozhong@snnu.edu.cn; Zhang Xue-Peng, Tel: (86)18673782167; E-mail: zhangxp@snnu.edu.cn; Cao Rui, Tel: (86-29) 81530726, E-mail: ruicao@snnu.edu.cn.

strong electron-withdrawing substituents showed an ORR half-wave potential of $E_{1/2}$ = 0.76 V versus reversible hydrogen electrode (RHE) in 0.1 mol·L^{-1} KOH solutions[44]. On the other hand, ORR happens at the liquid/gas/solid interface. Therefore, the hydrophilicity of catalysts should also play crucial roles in determining the activity[45, 46]. Based on these considerations, we are interested in examining the ORR activity of Co porphyrins by fine-tuning electronic structure and hydrophilic property of the meso-substituents.

Herein, we report on Co porphyrins, NO_2-CoP and 5F-CoP, and their electrocatalytic ORR features. NO_2-CoP is more efficient than 5F-CoP for electrocatalytic ORR by displaying a 60-mV anodic shift of the ORR half-wave potential. Compared with 5F-CoP, complex NO_2-CoP is more hydrophobic. Theoretical calculations suggest that NO_2-CoP is also more efficient than 5F-CoP to bind with an O_2 molecule to form Co^{III}-$O_2^{\bullet-}$. This work therefore presents a simple but an effective strategy to improve catalytic ORR activity by introducing electron-withdrawing and hydrophilic substituents to molecular catalysts.

2 Experimental Section

2.1 Syntheses of CoII Porphyrins (5F-CoP and NO_2-CoP)

Synthesis of 5F-CoP[47]. Pyrrole(670 mg, 10 mmol) and pentafluorobenzaldehyde (1.96 g, 10 mmol) were added into acetic acid (100 mL). After stirring for 4 h at 140 ℃, the mixture was then dried in vacuum to remove acetic acid. The residue was then purified on a silica column to give a purple solid of tetrakis (pentafluorophenyl)porphyrin (365.7 mg; yield 15%). Co acetate tetrahydrate (2.99 g, 12 mmol) and tetrakis (pentafluorophenyl)porphyrin (365.7 mg, 0.38 mmol) were added into a mixture of DMF (30 mL) and $CHCl_3$ (6 mL). The mixture was stirred at 120 ℃ with reflux for 12 h. After that, the mixture was rinsed with H_2O (150 mL) and then was dried with $MgSO_4$. Further purification by column chromatography gave the purple solid product of 5F-CoP (360.6 mg; yield 92%). Single crystals of 5F-CoP were obtained by slow evaporation of a mixed solution of 5F-CoP in methanol and chloroform (v:v = 1:1).

Synthesis of NO_2-CoP. Pyrrole(670 mg, 10 mmol) and 4-nitrobenzaldehyde (1.51 g, 10 mmol) were added into acetic acid (100 mL). After stirring for 0.5 h at 140 ℃, the mixture was then dried in vacuum to remove acetic acid, and was then recrystallized from acetone. The resulted solid was added into pyridine with reflux for 1.5 h. The mixture was dried in vacuum to remove pyridine and then dried in vacuum again to give a purple solid of tetrakis(4-nitrophenyl) porphyrin (319.1 mg; yield 15%). Co acetate tetrahydrate (747.2 mg, 3 mmol) and tetrakis(4-nitrophenyl) porphyrin (79.4 mg, 0.1 mmol) were added into DMF (15 mL). The mixture was stirred at 120 ℃ with reflux for 12 h. After that, the mixture was rinsed with H_2O (150 mL) and then was dried with $MgSO_4$. Further purification by column chromatography gave the purple solid product of NO_2-CoP (63.5 mg; yield 75%). Single crystals of NO_2-CoP were obtained by slow vapor diffusion of n-heptane to the NO_2-CoP solution in tetrahydrofuran.

2.2 Characterizations

Complete data sets for the NO_2-CoP (CCDC 2036420) and 5F-CoP (CCDC 2150347) were collected on an X-ray diffractometer (D8 VENTURE, Bruker). Single crystals suitable for X-ray analysis were coated with Paratone-N oil, suspended in a small fiber loop, and placed in a cooled gas stream at 153(2) K. Diffraction intensities were measured using Mo K_α radiation (λ = 0.71073Å). Data collection, indexing, reduction, and unit cell refinements were carried out using APEX2[48]. Absorption corrections were applied using the program SADABS[49]. The single crystal structure was solved with direct methods using SHELXS[50] and refined against F^2 on all data by full-matrix least squares with SHELXL-97[51] following established refinement strategies. All non-hydrogen atoms were refined anisotropically. All hydrogen atoms binding to carbon are included in the model at geometrically calculated positions and refined using a riding model. The isotropic displacement parameters of all hydrogen atoms are fixed to 1.2 times the U value of atoms they are linked to. Details of data

quality and a summary of residual values of refinements are given in Table S1 for NO_2-CoP and Table S2 for 5F-CoP.

UV-vis spectra were collected using a spectrophotometer (U-3310, Hitachi). ^{1}H NMR spectra were acquired on a spectrometer operating at 400 MHz (Bruker). High resolution mass spectra (HRMS) were measured using high resolution liquid chromatography mass spectrometry (Bruker). For electrocatalytic measurements, Co porphyrins were directly loaded on carbon nanotubes (CNTs). Morphologies of catalyst@CNT hybrids were measured with a scanning electron microscope (SEM, SU8020, Hitachi) and transmission electron microscope (TEM, Tecnai G2 F20, FEI). X-ray photoelectron spectroscopic (XPS) results were measured with an XPS (Thermo ESCALAB 250XI). Hydrophilicities were measured with a video-based contact angle instrument (OCA 20, Dataphysics) for three times to obtain average values. Co porphyrin molecules and the catalyst inks were coated on the silicon slice with the same loading on the electrode.

2.3 Electrochemical Tests

Electrocatalytic ORR measurements were carried out with a CHI 760E electrochemical workstation and a Pine Modulated Speed Rotator in 0.1 mol·L^{-1} KOH with a typical three-electrode system. Rotating disk electrode (RDE, 0.196 cm^2), carbon rod, and saturated Ag/AgCl electrode were used as the working electrode, auxiliary electrode, and reference electrode, respectively. To prepare catalyst ink, the 5F-CoP (1 mmol) or NO_2-CoP (1 mmol) and CNTs (1 mg) were added into DMF (1 mL) with 20 μL Nafion (5wt%, DuPont). Commercial CNTs (> 95% purity, < 8 nm outside diameter, 3 nm inside diameter) were used in this work. The resulting mixture was sonicated for 1 h to obtain a catalyst ink. Typically, 20 μL of catalyst ink was coated onto RDE to form a catalyst film. The catalyst loadings of 5F-CoP/CNT and NO_2-CoP/CNT were 0.21 and 0.19 mg·cm^{-2}, respectively. The DMF solvent, after dropping the catalyst ink on the electrode, was volatilized slowly and completely in 12 h at room temperature. Linear sweep voltammogram (LSV) was measured in O_2-saturated 0.1 mol·L^{-1} KOH at 5 mV·s^{-1} and 1600 r·min^{-1}. The potential between Ag/AgCl electrode and RHE is calculated according to Equation 1.

$$E_{RHE} = E_{Ag/AgCl} + 0.197 + 0.059 \times pH \text{ (V)} \quad (1)$$

Tafel slopes were calculated by measuring LSV data at 2 mV·s^{-1} and 1600 r·min^{-1}. The number (n) of electrons transferred per O_2 molecule was calculated by measuring LSV with rotating ring-disk electrode (RRDE; disk: 0.247 cm^2, ring: 0.186 cm^2) at 5 mV·s^{-1} and 1600 r·min^{-1}. The n is calculated with Equation 2.

$$n = 4\frac{i_d}{i_d + i_r/N} \quad (2)$$

Herein, i_d is the disk current, i_r is the ring current, and N is the collection efficiency of ring current (0.39). The n was also calculated based on Koutecky-Levich (K-L) equations (3 and 4) by measuring LSV data at different rotating speeds.

$$\frac{1}{J} = \frac{1}{J_L} + \frac{1}{J_K} = \frac{1}{B\omega^{1/2}} + \frac{1}{J_K} \quad (3)$$

$$B = 0.2nFC_0D_0^{2/3}\upsilon^{-1/6} \quad (4)$$

Herein, J is the current density measured with LSV, J_L is the diffusion-limited J, J_K is the kinetic-limited J, ω is the angular velocity, F is the Faraday constant (96485 C·mol^{-1}), C_0 is the bulk concentration of O_2 (1.2×10^{-3} mol·L^{-1}), D_0 is the diffusion coefficient of O_2 (1.9×10^{-5} cm^2·s^{-1}) and υ is the kinematic viscosity of electrolyte (1.0×10^{-2} cm^2·s^{-1})[52].

2.4 Theoretical Calculations

Density functional theory (DFT) calculation results are obtained with Gaussian 16 program[53]. Geometry optimization and harmonic frequency are conducted with D3BJ[54]-B3LYP[55-57]/Def2-SVP[58]. Single-point energy refinement in an aqueous solution are conducted at the level of D3BJ-B3LYP/Def2-TZVP with polarized continuum model (PCM)[59] and integral equation formalism PCM (IEFPCM). Atomic charges conducted natural population analysis (NPA)[60] are utilized. All thermodynamic data are reported under 298.15 K and 1 atm.

3 Results and Discussion

3.1 Synthesis and Characterization

Porphyrin ligands and the corresponding Co porphyrins (Figure 1a and 1b) were synthesized. Their

identity and purity were confirmed by ^{1}H NMR and HRMS (Figure S1-S4). Complex 5F-CoP displayed an ion with a mass-to-charge ratio of 1030.9750, which is consistent with the calculated value of 1030.9756 (Figure S2). Complex NO_2-CoP displayed an ion with a mass-to-charge ratio of 851.1031, matching well with the calculated value of 851.1044 (Figure S4). Single crystal X-ray structures of NO_2-CoP and 5F-CoP were obtained, further confirming the formation of these Co porphyrins (Figure 1c and 1d). Crystallographic studies reveal that the NO_2-CoP crystallized in the monoclinic space group $P2_1/c$ with a = 10.8572(9) Å, b = 16.7957(13) Å, c = 13.2241(10) Å, and β = 109.280(3)° (Table S1), while the 5F-CoP crystallized in the orthorhombic space group *Pnnm* with a = 7.3850(8) Å, b = 14.4400(14) Å, c = 24.902 (3) Å (Table S2). In both NO_2-CoP and 5F-CoP, the Co ions are coordinated by the corresponding porphyrin ligand through four N atoms, leading to the same Co-N_4 square-planar coordination structure. The average Co-N bond distance is 1.974(3) Å for NO_2-CoP and 1.991(3) Å for 5F-CoP. Furthermore, the plane of both pentafluorobenzene and 4-nitrobenzene substituents is perpendicular to the plane of their porphyrin macrocycles. These results showed that the coordination structures of the Co ions with NO_2-CoP and 5F-CoP are similar to each other.

Cyclic voltammogram of Co porphyrins in 0.1 mol·L^{-1} $Bu_4N(PF_6)$ DMF solution under N_2 was measured (Figure S5). The redox peaks of Co^{II}/Co^{I} and Co^{I}/Co^{0} for the 5F-CoP appeared at -1.12 V and -2.14 V (vs. ferrocene), respectively. Similarly, the cyclic voltammtric (CV) curve of NO_2-CoP displayed peaks at -1.14 V and -2.38 V (vs. ferrocene) corresponding to redox potentials of Co^{II}/Co^{I} and Co^{I}/Co^{0}, respectively. The peaks appeared at -1.54 V (vs. ferrocene) is attributed to the redox features of the nitrobenzene substituents. The Co porphyrins were then loaded on the CNTs for electrocatalytic ORR measurements (Figure 2a). The resulted molecule/CNT hybrids were named as NO_2-CoP/CNT and 5F-CoP/CNT. Compared with the unmodified CNTs (Figures S6 and S7), no obvious changes were observed for the NO_2-CoP/CNT (Figure 2b and 2c) by scanning electron microscopy (SEM) and transmission electron microscopy (TEM), indicating the absence of aggregated Co porphyrin particles in the hybrid. Scanning TEM and element distribution images of Co, N, and O showed that NO_2-CoP molecules were evenly loaded on CNTs (Figure 2d). Similar results were also obtained for the 5F-CoP/CNT.

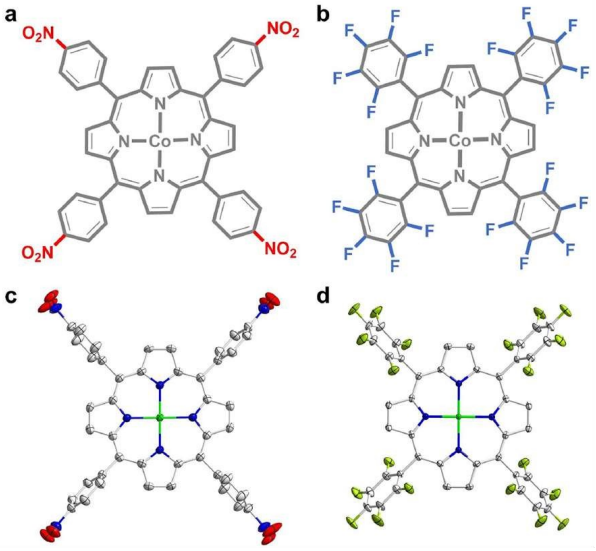

Figure 1 Molecular structures (a, b) and thermal ellipsoid plots (50% probability) of the X-ray crystal structures (c, d) of NO_2-CoP and 5F-CoP. Color codes: green Co, red O, blue N, yellow green F, white C. (color on line)

X-ray photoelectron spectroscopic (XPS) analysis of these hybrids was made to further confirm the existence of Co porphyrins (Figure S8). From high resolution XPS spectra of Co 2p, two weak but characteristic peaks at 780.1 and 795.6 eV were observed for both hybrids (Figure 2e), demonstrating the formation of molecule/CNT catalysts. In addition, the NO_2-CoP/CNT showed XPS signal of O 1s at 533.4 eV (Figure 2f), while the 5F-CoP/CNT exhibited XPS peak of F 1s at 688.4 eV (Figure 2g). XPS peak appeared at 286.6 eV of C 1s for the NO_2-CoP/CNT further confirmed the existence of C-N bond (Figure S9). All XPS results above confirmed the successful preparation of molecule/CNT hybrids.

3.2 Electrocatalytic ORR Studies

The activity and selectivity of molecule/CNT

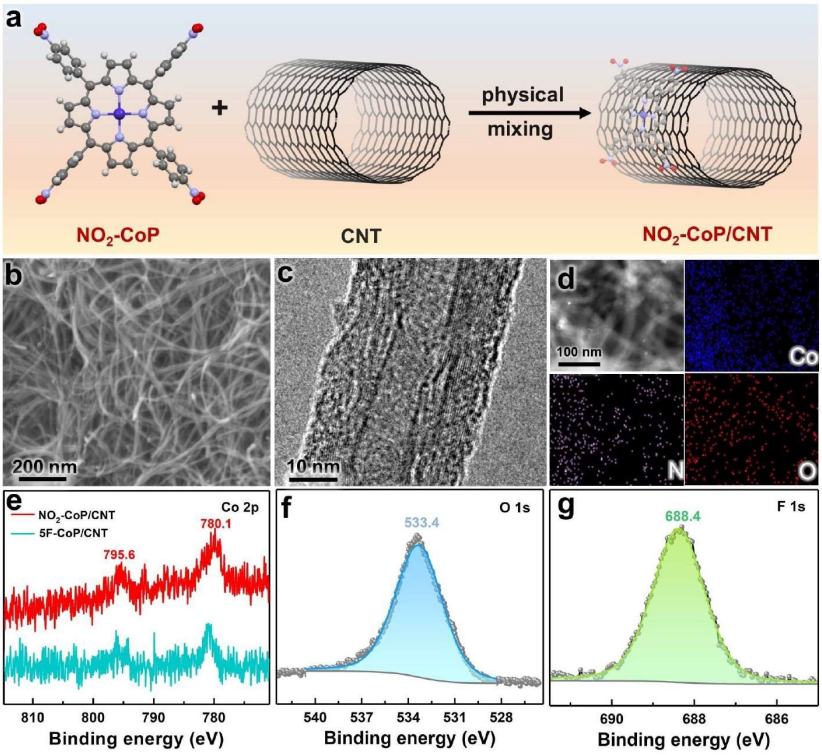

Figure 2 (a) Preparation of molecule/CNT hybrids. (b) SEM image, (c) TEM image, (d) scanning TEM and corresponding elemental images of NO_2-CoP/CNT. (e) XPS spectra of Co 2p for NO_2-CoP/CNT and 5F-CoP/CNT. (f) XPS spectrum of O 1s for NO_2-CoP/CNT. (g) XPS spectrum of F 1s for 5F-CoP/CNT. (color on line)

hybrids for ORR were evaluated in 0.1 mol·L^{-1} KOH aqueous solutions (Figure 3). The CV curve of NO_2-CoP/CNT showed large catalytic currents under O_2 (Figure 3a), indicating its electrocatalytic activity for ORR. The ORR peak potential with the NO_2-CoP/CNT (0.74 V) was more positive than that of the 5F-CoP/CNT (0.69 V) (Figure S10). The LSV curves of molecule/CNT hybrids, CNTs and commercial Pt/C (20wt%) were measured at 1600 r·min^{-1} with a rotating ring-disk electrode (RRDE). The $E_{1/2}$ value of the NO_2-CoP/CNT was 0.82 V (versus RHE) (Figure 3b), while the $E_{1/2}$ value of the 5F-CoP/CNT was 0.76 V (versus RHE). Note that the commercial Pt/C (20wt%) exhibited an $E_{1/2}$ value of 0.88 V (versus RHE). The ORR performance of blank RDE was negligible (Figure S11). The ORR performance of NO_2-CoP/CNT was remarkable compared with many other porphyrin based molecular catalysts reported in the literature (Table S3). It is worth noting that both NO_2-CoP/ CNT and 5F-CoP/CNT are more active than the unmodified CNTs ($E_{1/2}$ = 0.72 V versus RHE) for electrocatalytic ORR. The ORR Tafel slope of NO_2-CoP/CNT (31 mV·dec^{-1}) was smaller than that of 5F-CoP/CNT (44 mV·dec^{-1}) (Figure 3c). Tafel slopes of CNT and Pt/C were 55 and 70 mV·dec^{-1}, respectively.

In addition, the number (n) of electrons transferred for ORR was determined with the RRDE measurements, giving n = 3.19 for the 5F-CoP/CNT and n = 3.10 for the NO_2-CoP/CNT (Figure 3d). Similar n values were also obtained by using Koutecky-Levich (K-L) analysis (Figure 3e and 3f)[38]. Therefore, the 5F-CoP/CNT and NO_2-CoP/CNT displayed similar selectivity for ORR.

3.3 Electronic Structures and Hydrophilicity

The UV-vis spectrum of NO_2-CoP under N_2 showed characteristic Soret and Q bands at 420 and 531 nm, respectively (Figure 4a). Similar spectrum of 5F-CoP under N_2 was obtained with Soret and Q bands at 410 and 526 nm, respectively (Figure 4b). The UV-vis spe-

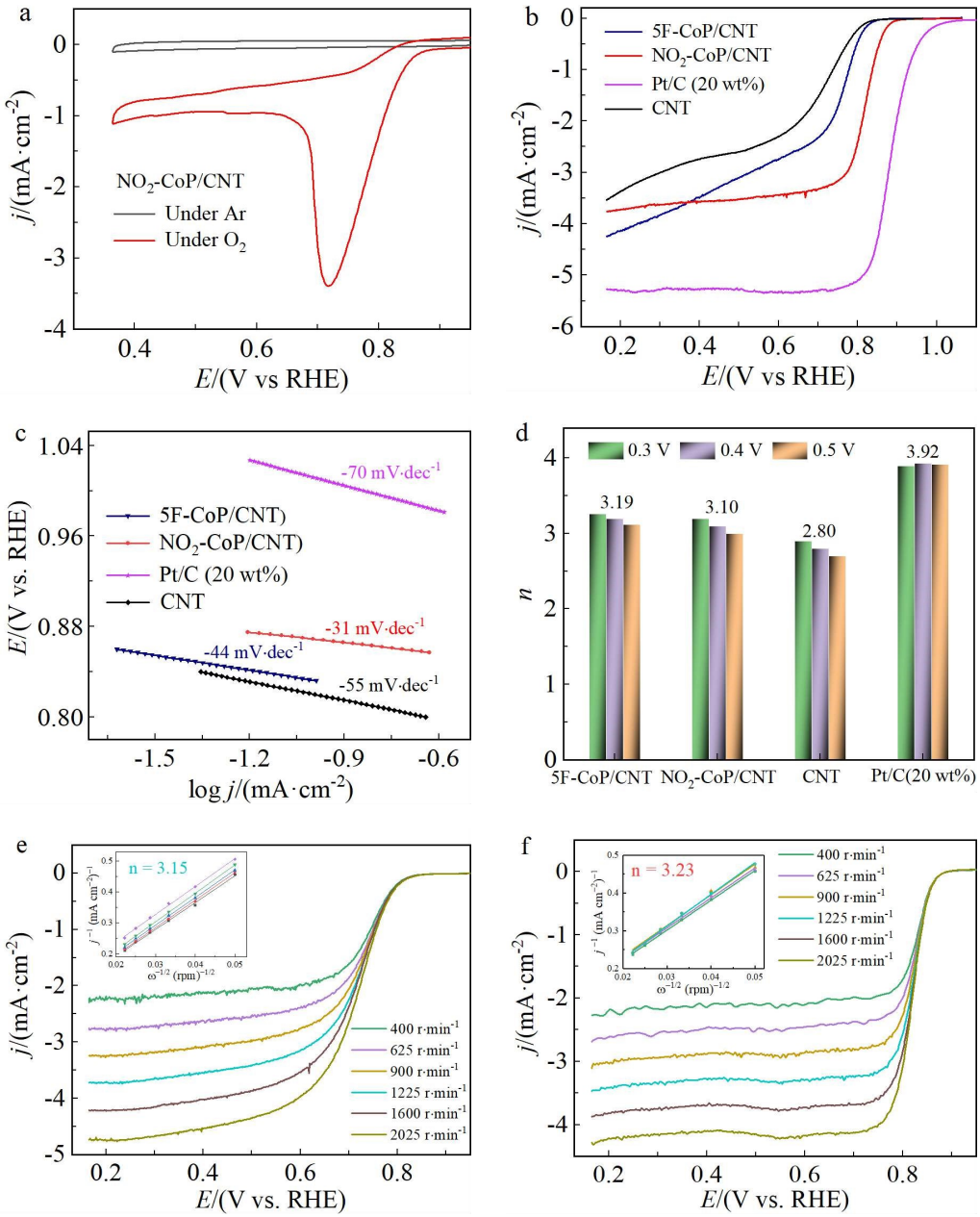

Figure 3 (a) CV curves of NO_2-CoP/CNT under argon and O_2. (b) LSV curves, (c) Tafel plots, and (d) *n* values of 5F-CoP/CNT, NO_2-CoP/CNT, CNTs and Pt/C(20wt%) for electrocatalytic ORR in 0.1 mol·L^{-1} KOH. Conditions: RRDE, 5 mV·s^{-1}, and 1600 r·min^{-1}. LSVs at different rotating speeds and Koutecky-Levich plots with *n* values of 5F-CoP/CNT (e) and NO_2-CoP/CNT (f). (color on line)

ctrum of NO_2-CoP under O_2 displayed new peaks at 429 nm and 540 nm in 30 min (Figure S12), indicating the formation of Co^{III}-$O_2^{\bullet-}$ species[18]. However, unlike NO_2-CoP, the UV-vis spectrum of 5F-CoP under O_2 displayed no obvious changes compared to that under N_2. These results suggested that the NO_2-CoP is more efficient than the 5F-CoP to bind with O_2.

Complex NO_2-CoP had a good hydrophilicity by featuring a small contact angle of 8.6° (Figure 5a). In contrast, 5F-CoP was much more hydrophobic by displaying a large contact angle of 111.4° (Figure 5b). The contact angles of CNTs and molecule/CNT hybrids were also measured. The CNTs were hydrophobic with a large contact angle of 138.5° (Figure S13). The contact angles of NO_2-CoP/CNT and 5F-CoP/CNT hybrids were 121.3° and 136.6°, re-

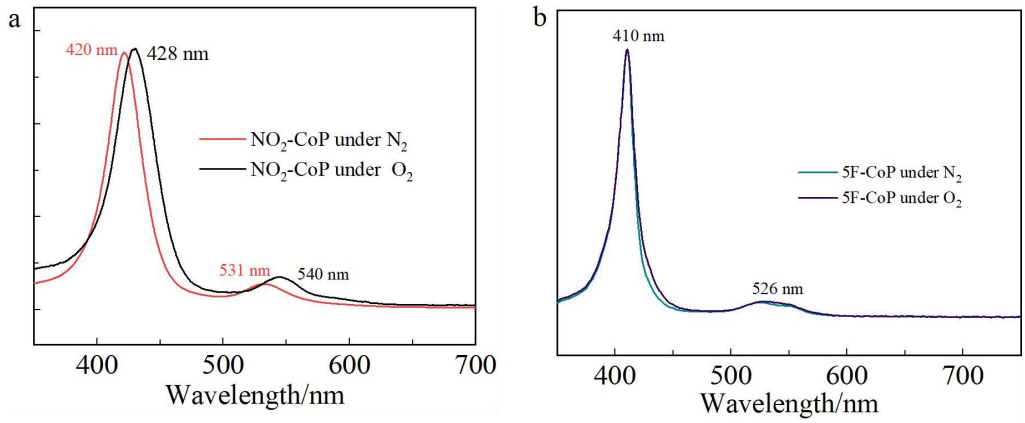

Figure 4 UV-vis spectra of (a) NO_2-CoP and (b) 5F-CoP measured under N_2 and O_2. (color on line)

spectively (Figure 5c and 5d). These results showed that after loading on CNTs, the resulted NO_2-CoP/CNT is still more hydrophilic than 5F-CoP/CNT.

3.4 Theoretical Calculations

The ORR processes associated with the NO_2-CoP/CNT and 5F-CoP/CNT were also investigated by using DFT calculations. As shown in Figure 6a, starting from the Co^{II} state, Co porphyrins are considered to bind with an O_2 molecule to afford Co^{III}-$O_2^{\bullet-}$. Herein, the O_2 binding process is calculated to have proper association free energies (ΔG_1). Importantly, the ΔG_1 value of NO_2-CoP (14.3 kcal·mol^{-1}) is smaller than that of 5F-CoP (18.6 kcal·mol^{-1}), demonstrating that NO_2-CoP is more efficient to bind with O_2. This result is consistent with the findings observed during the UV-vis measurements of NO_2-CoP and 5F-CoP. In addition, the spin density distributions of Co^{III}-$O_2^{\bullet-}$ are analysed (Figure 6b and 6c). The Co^{III}-O bond length in the Co^{III}-$O_2^{\bullet-}$ form of NO_2-CoP is 1.86 Å, while that of 5F-CoP is 1.859 Å. The similar Co^{III}-O bond length is attributed to the similar electron-withdrawing features of NO_2- and F-substituents. However, the O-O bond length in the Co^{III}-$O_2^{\bullet-}$ form of NO_2-CoP (1.251 Å) is larger than that of 5F-CoP (1.248 Å), demonstrating the improved O_2 activation with NO_2-CoP as compared with that with 5F-CoP. To conclude,

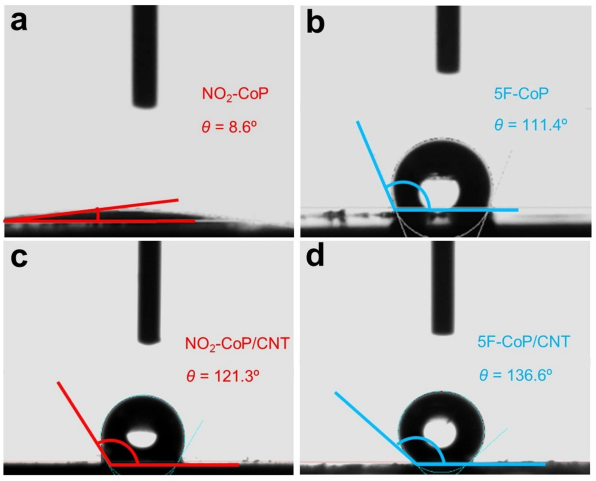

Figure 5 Contact angles of (a) NO_2-CoP, (b) 5F-CoP, (c) NO_2-CoP/CNT, and (d) 5F-CoP/CNT. (color on line)

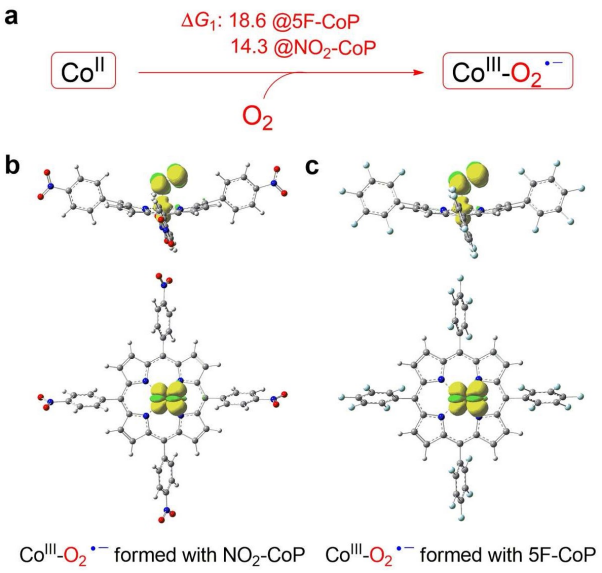

Figure 6 (a) O_2 binding with Co porphyrins (free energies reported in kcal·mol^{-1}). Snapshots of spin density distribution of Co^{III}-$O_2^{\bullet-}$ formed with NO_2-CoP (b) and 5F-CoP (c) from the side view and top view. (color on line)

with fine-tuned electronic structures, NO_2-CoP outperformes over 5F-CoP for O_2 activation, which is consis tent with the experimental results.

4 Conclusions

In summary, we reported on two Co porphyrins, NO_2-CoP and 5F-CoP, and their electrocatatlytic ORR features. By fine-tuning the electronic structure and hydrophilic feature, the NO_2-CoP displayed significnatly imporved ORR activity compared with the 5F-CoP. Importantly, the NO_2-CoP exhibited an $E_{1/2}$ value of 0.82 V (versus RHE), making it one of the most efficient moleculr ORR electrocatalysts in literature. Results from both experimental and theoretical studies suggested that NO_2-CoP is more efficient than 5F-CoP to bind with O_2. Therefore, this work provides a strategy to use substituents to fine-tune the electronic structure and hydrophilic feature of molecular catalysts for improved ORR.

Acknowledgements:

Authors are grateful for supports from National Natural Science Foundation of China (22178213, 21773146, 22171176, and 22003036), Fundamental Research Funds for the Central Universities (GK 202103029 and GK202103045), Key Research and Development Program of Shaanxi (2022GY-196), and Young Talent fund of University Association for Science and Technology in Shaanxi, China (20200602).

References:

[1] Zaman S, Huang L, Douka A I, Yang H, You B, Xia B Y. Oxygen reduction electrocatalysts toward practical fuel cells: Progress and perspectives[J]. Angew. Chem. Int. Ed., 2021, 60(33): 17832-17852.

[2] Zhao C X, Liu J N, Wang J, Ren D, Li B Q, Zhang Q. Recent advances of noble-metal-free bifunctional oxygen reduction and evolution electrocatalysts[J]. Chem. Soc. Rev., 2021, 50(13): 7745-7778.

[3] Amanullah S, Das P K, Samanta S, Dey A. Tuning the thermodynamic onset potential of electrocatalytic O_2 reduction reaction by synthetic iron-porphyrin complexes[J]. Chem. Commun., 2015, 51(49): 10010-10013.

[4] Kong J F, Cheng W L. Recent advances in the rational design of electrocatalysts towards the oxygen reduction reaction[J]. Chin. J. Catal., 2017, 38(6): 951-969.

[5] Song P, Ruan M B, Liu J, Ran G J, Xu W L. Recent research progress for non-Pt-based oxygen reduction reaction electrocatalysts in fuel cell[J]. J. Electrochem., 2015, 21 (2): 130-137.

[6] Wang D, Pan X N, Yang P X, Li R P, Xu H, Li Y, Meng F, Zhang J Q, An M Z. Transition metal and nitrogen Co-doped carbon-based electrocatalysts for the oxygen reduction reaction: From active site insights to the rational design of precursors and structures[J]. ChemSusChem, 2021, 14(1): 33-55.

[7] Zhao T, Luo E G, Wang X, Ge J J, Liu C P, Xing W. Challenges in the activity and stability of Pt-based catalysts toward ORR[J]. J. Electrochem., 2020, 26(1): 84-95.

[8] Kumar A, Zhang Y, Jia Y, Liu W, Sun X M. Redox chemistry of N_4-Fe^{2+} in iron phthalocyanines for oxygen reduction reaction[J]. Chin. J. Catal., 2021, 42(8): 1404-1412.

[9] Fukuzumi S, Lee Y M, Nam W. Recent progress in production and usage of hydrogen peroxide[J]. Chin. J Catal., 2021, 42(8): 1241-1252.

[10] Dey S, Mondal B, Chatterjee S, Rana A, Amanullah S K, Dey A. Molecular electrocatalysts for the oxygen reduction reaction[J]. Nat. Rev. Chem., 2017, 1(12): 0098.

[11] Pegis M L, Wise C F, Martin D J, Mayer J M. Oxygen reduction by homogeneous molecular catalysts and electrocatalysts[J]. Chem. Rev., 2018, 118(5): 2340-2391.

[12] Zhang W, Lai W Z, Cao R. Energy-related small molecule activation reactions: Oxygen reduction and hydrogen and oxygen evolution reactions catalyzed by porphyrin- and corrole-based systems[J]. Chem. Rev., 2017, 117(4): 3717-3797.

[13] Passard G, Dogutan D K, Qiu M T, Costentin C, Nocera D G. Oxygen reduction reaction promoted by manganese porphyrins[J]. ACS Catal., 2018, 8(9): 8671-8679.

[14] Zhao Y M, Yu G Q, Wang F F, Wei P J, Liu J G. Bioinspired transition-metal complexes as electrocatalysts for the oxygen reduction reaction[J]. Chem. Eur. J., 2019, 25 (15): 3726-3739.

[15] Zhou Y, Xing Y F, Wen J, Ma H B, Wang F B, Xia X H. Axial ligands tailoring the ORR activity of cobalt porphyrin[J]. Sci. Bull., 2019, 64(16): 1158-1166.

[16] Xie L S, Zhang X P, Zhao B, Li P, Qi J, Guo X N, Wang B, Lei H T, Zhang W, Apfel U P, Cao R. Enzyme-inspired iron porphyrins for improved electrocatalytic oxygen reduction and evolution reactions[J]. Angew. Chem. Int. Ed., 2021, 60(14): 7576-7581.

[17] Lv H Y, Guo H B, Guo K, Lei H T, Zhang W, Zheng H Q, Liang Z Z, Cao R. Substituent position effect of Co porphyrin on oxygen electrocatalysis[J]. Chin. Chem. Lett., 2021, 32(9): 2841-2845.

[18] Lv B, Li X L, Guo K, Ma J, Wang Y Z, Lei H T, Wang F,

Jin X T, Zhang Q X, Zhang W, Long R, Xiong Y J, Apfel U P, Cao R. Controlling oxygen reduction selectivity through steric effects: Electrocatalytic two-electron and four-electron oxygen reduction with cobalt porphyrin atropisomers[J]. Angew. Chem. Int. Ed., 2021, 60(23): 12742-12746.

[19] Hong Y H, Han J W, Jung J, Nakagawa T, Lee Y M, Nam W, Fukuzumi S. Photocatalytic oxygenation reactions with a cobalt porphyrin complex using water as an oxygen source and dioxygen as an oxidant[J]. J. Am. Chem. Soc., 2019, 141(23): 9155-9159.

[20] Li X L, Lei H T, Xie L S, Wang N, Zhang W, Cao R. Metalloporphyrins as catalytic models for studying hydrogen and oxygen evolution and oxygen reduction reactions[J]. Acc. Chem. Res., 2022, 55(6): 878-892.

[21] Zhang R, Warren J J. Recent developments in metalloporphyrin electrocatalysts for reduction of small molecules: Strategies for managing electron and proton transfer reactions[J]. ChemSusChem, 2021, 14(1): 293-302.

[22] Mondal B, Sen P, Dey A. Proton reduction in the presence of oxygen by iron porphyrin enabled with 2nd sphere redox active ferrocenes[J]. Chin. J. Catal., 2021, 42(8): 1327-1331.

[23] Grinstaff M W, Hill M G, Labinger J A, Gray H B. Mechanism of catalytic oxygenation of alkanes by halogenated iron porphyrins[J]. Science, 1994, 264(5163): 1311-1313.

[24] Zagal J H, Recio F J, Gutierrez C A, Zuniga C, Paez M A, Caro C A. Towards a unified way of comparing the electrocatalytic activity MN_4 macrocyclic metal catalysts for O_2 reduction on the basis of the reversible potential of the reaction[J]. Electrochem. Commun., 2014, 41: 24-26.

[25] Li Y L, Wang N, Lei H T, Li X L, Zheng H Q, Wang H Y, Zhang W, Cao R. Bioinspired N_4-metallomacrocycles for electrocatalytic oxygen reduction reaction[J]. Coord. Chem. Rev., 2021, 442: 213996.

[26] Masa J, Schuhmann W. Systematic selection of metalloporphyrin-based catalysts for oxygen reduction by modulation of the donor-acceptor intermolecular hardness[J]. Chem. Eur. J., 2013, 19(29): 9644-9654.

[27] Zhao C X, Li B Q, Liu J N, Huang J Q, Zhang Q. Transition metal coordinated framework porphyrin for electrocatalytic oxygen reduction[J]. Chin. Chem. Lett., 2019, 30(4): 911-914.

[28] Wang Y H, Mondal B, Stahl S S. Molecular cobalt catalysts for O_2 reduction to H_2O_2: Benchmarking catalyst performance via rate-overpotential correlations[J]. ACS Catal., 2020, 10(20): 12031-12039.

[29] Lei H T, Zhang Q X, Wang Y B, Gao Y M, Wang Y Z, Liang Z Z, Zhang W, Cao R. Significantly boosted oxygen electrocatalysis with cooperation between cobalt and iron porphyrins dagger[J]. Dalton Trans., 2021, 50(15): 5120-5123.

[30] Liu Y J, Zhou G J, Zhang Z Y, Lei H T, Yao Z, Li J F, Lin J, Cao R. Significantly improved electrocatalytic oxygen reduction by an asymmetrical pacman dinuclear cobalt(II) porphyrin-porphyrin dyad[J]. Chem. Sci., 2020, 11(1): 87-96.

[31] Oldacre A N, Friedman A E, Cook T R. A self-assembled cofacial cobalt porphyrin prism for oxygen reduction catalysis[J]. J. Am. Chem. Soc., 2017, 139(4): 1424-1427.

[32] Zhang W, Shaikh A U, Tsui E Y, Swager T M. Cobalt porphyrin functionalized carbon nanotubes for oxygen reduction[J]. Chem. Mater., 2009, 21(14): 3234-3241.

[33] Liang Z Z, Guo H B, Zhou G J, Guo K, Wang B, Lei H T, Zhang W, Zheng H Q, Apfel U P, Cao R. Metal-organic-framework-supported molecular electrocatalysis for the oxygen reduction reaction[J]. Angew. Chem. Int. Ed., 2021, 60(15): 8472-8476.

[34] Crawley M R, Zhang D Y, Oldacre A N, Beavers C M, Friedman A E, Cook T R. Tuning the reactivity of cofacial porphyrin prisms for oxygen reduction using modular building blocks[J]. J. Am. Chem. Soc., 2021, 143(2): 1098-1106.

[35] Wan H, Jensen A W, Escudero-Escribano M, Rossmeisl J. Insights in the oxygen reduction reaction: From metallic electrocatalysts to diporphyrins[J]. ACS Catal., 2020, 10(11): 5979-5989.

[36] Sun B, Ou Z P, Meng D Y, Fang Y Y, Song Y, Zhu W H, Solntsev P V, Nemykin V N, Kadish K M. Electrochemistry and catalytic properties for dioxygen reduction using ferrocene-substituted cobalt porphyrins[J]. Inorg. Chem., 2014, 53(16): 8600-8609.

[37] Zhang Q X, Wang Y B, Wang Y Z, Yang S J, Wu X, Lv B, Wang N, Gao Y M, Xu X R, Lei H T, Cao R. Electropolymerization of cobalt porphyrins and corroles for the oxygen evolution reaction[J]. Chin. Chem. Lett., 2021, 32(12): 3807-3810.

[38] Song E H, Shi C N, Anson F C. Comparison of the behavior of several cobalt porphyrins as electrocatalysts for the reduction of O_2 at graphite electrodes[J]. Langmuir, 1998, 14(15): 4315-4321.

[39] Xie L S, Li X L, Wang B, Meng J, Lei H T, Zhang W, Cao R. Molecular engineering of a 3D self-supported electrode for oxygen electrocatalysis in neutral media[J]. Angew. Chem. Int. Ed., 2019, 58(52): 18883-18887.

[40] Han J X, Wang N, Li X L, Zhang W, Cao R. Improving

electrocatalytic oxygen reduction activity and selectivity with a cobalt corrole appended with multiple positively charged proton relay sites[J]. J. Phys. Chem. C, 2021, 125 (45): 24805-24813.

[41] Sonkar P K, Prakash K, Yadav M, Ganesan V, Sankar M, Gupta R, Yadav D K. Co(II)-porphyrin-decorated carbon nanotubes as catalysts for oxygen reduction reactions: An approach for fuel cell improvement[J]. J. Mater. Chem. A, 2017, 5(13): 6263-6276.

[42] McGuire R, Dogutan D K, Teets T S, Suntivich J, Shao-Horn Y, Nocera D G. Oxygen reduction reactivity of cobalt(II) hangman porphyrins[J]. Chem. Sci., 2010, 1(3): 411-414.

[43] Liang Z, Wang H Y, Zheng H Q, Zhang W, Cao R. Porphyrin-based frameworks for oxygen electrocatalysis and catalytic reduction of carbon dioxide[J]. Chem. Soc. Rev., 2021, 50(4): 2540-2581.

[44] Qin H N, Wang Y Z, Wang B, Duan X G, Lei H T, Zhang X P, Zheng H Q, Zhang W, Cao R. Cobalt porphyrins supported on carbon nanotubes as model catalysts of metal-N_4/C sites for oxygen electrocatalysis[J]. J. Energy Chem., 2021, 53: 77-81.

[45] Xu W W, Lu Z Y, Sun X M, Jiang L, Duan X. Superwetting electrodes for gas-involving electrocatalysis[J]. Acc. Chem. Res., 2018, 51(7): 1590-1598.

[46] Longhi M, Cova C, Pargoletti E, Coduri M, Santangelo S, Patanè S, Ditaranto N, Cioffi N, Facibeni A, Scavini M. Synergistic effects of active sites' nature and hydrophilicity on the oxygen reduction reaction activity of Pt-free catalysts[J]. Nanomaterials, 2018, 8(9): 643.

[47] Lei H T, Wang Y B, Zhang Q X, Cao R. First-row transition metal porphyrins for electrocatalytic hydrogen evolution — a SPP/JPP Young Investigator Award paper[J]. J. Porphyr. Phthalocyanines, 2020, 24(11-12): 1361-1371.

[48] Brüker AXS. APEX2 V2009.

[49] Sheldrick G. SADABS—Brüker AXS area detector scaling and absorption, version 2008/1. University of Göttingen, Germany, 2008.

[50] Sheldrick G M. Phase annealing in SHELX-90: Direct methods for larger structures[J]. Acta Cryst., 1990, 46: 467-473.

[51] Sheldrick G M. Crystal structure refinement with SHEL XL[J]. Acta Cryst., 2015, 71: 3-8.

[52] Xia B Y, Yan Y, Li N, Wu H B, Lou X W, Wang X. A metal-organic framework-derived bifunctional oxygen electrocatalyst[J]. Nat. Energy, 2016, 1: 15006.

[53] Frisch M J, Trucks G W, Schlegel H B, Scuseria G E, Robb M A, Cheeseman J R, Fox D J. Gaussian16 Revision A. 03 (Wallingford, Ct: Gaussian Inc.), 2016.

[54] Grimme S, Ehrlich S, Goerigk L. Effect of the damping function in dispersion corrected density functional theory [J]. J. Comp. Chem., 2011, 32(7): 1456-1465.

[55] Becke A D. Density-functional exchange-energy approximation with correct asymptotic behavior[J]. Phys. Rev. A, 1988, 38(6): 3098-3100.

[56] Lee C T, Yang W T, Parr R G. Development of the colle-salvetti correlation-energy formula into a functional of the electron density[J]. Phys. Rev. B, 1988, 37(2): 785-789.

[57] Becke A D. Density-functional thermochemistry. III. The role of exact exchange[J]. J. Chem. Phys., 1993, 98(7): 5648-5652.

[58] Weigend F, Ahlrichs R. Balanced basis sets of split valence, triple zeta valence and quadruple zeta valence quality for H to Rn: Design and assessment of accuracy [J]. Phys. Chem. Chem. Phys., 2005, 7(18): 3297-3305.

[59] Tomasi J, Mennucci B, Cammi R. Quantum mechanical continuum solvation models[J]. Chem. Rev., 2005, 105(8): 2999-3093.

[60] Reed A E, Curtiss L A, Weinhold F. Intermolecular interactions from a natural bond orbital, donor-acceptor viewpoint[J]. Chem. Rev., 1988, 88(6): 899-926.

吸电子和亲水性 Co-卟啉促进电催化氧还原反应的研究

郭鸿波[#],王亚妮[#],郭 凯,雷海涛,梁作中[*],张学鹏[*],曹 睿[*]

(陕西师范大学化学化工学院,应用表面与胶体化学教育部重点实验室, 陕西 西安 710119)

摘要: 研究影响电催化氧还原反应活性的因素对于合理设计高效的氧还原反应催化剂至关重要。调节催化剂电子结构通常被用于精确调控电催化氧还原反应活性。然而, 该反应发生在液/气/固界面, 很少有报道调控分子催化剂的亲疏水性来提高其催化活性。在此, 我们报道了两种钴卟啉 NO_2-CoP(5,10,15,20-四(4-硝基苯基)钴卟啉)和 5F-CoP(5,10,15,20-四(五氟苯基)钴卟啉)并研究了其电催化氧还原反应性能。通过同时调控 meso-位取代基的电子结构和亲水性能, NO_2-CoP 显示出比 5F-CoP 更高的电催化氧还原反应活性, 其半波电位向阳极方向移动近 60 mV。NO_2-CoP 比 5F-CoP 具有更好的亲水性。理论计算表明, NO_2-CoP 比 5F-CoP 更容易有效地与 O_2 分子结合形成 Co^{III}-$O_2^{\bullet-}$。这项工作提供了一个简单而有效的策略, 通过使用吸电子和亲水取代基来提高钴卟啉的氧还原反应活性。该策略对于设计和开发其他用于电催化的分子催化剂体系也具有重要的启发意义。

关键词: 分子电催化;氧还原反应;钴卟啉;亲水性;电子结构